Eddy-Driven Recirculations from a Localized Transient Forcing

STEPHANIE WATERMAN*

Massachusetts Institute of Technology–Woods Hole Oceanographic Institution Joint Program, Woods Hole, Massachusetts

STEVEN R. JAYNE

Woods Hole Oceanographic Institution, Woods Hole, Massachusetts

(Manuscript received 28 March 2011, in final form 22 September 2011)

ABSTRACT

The generation of time-mean recirculation gyres from the nonlinear rectification of an oscillatory, spatially localized vorticity forcing is examined analytically and numerically. Insights into the rectification mechanism are presented and the influence of the variations of forcing parameters, stratification, and mean background flow are explored. This exploration shows that the efficiency of the rectification depends on the properties of the energy radiation from the forcing, which in turn depends on the waves that participate in the rectification process. The particular waves are selected by the relation of the forcing parameters to the available free Rossby wave spectrum. An enhanced response is achieved if the parameters are such to select meridionally propagating waves, and a resonant response results if the forcing selects the Rossby wave with zero zonal group velocity and maximum meridional group velocity, which is optimal for producing rectified flows. Although formulated in a weakly nonlinear wave limit, simulations in a more realistic turbulent system suggest that this understanding of the mechanism remains useful in a strongly nonlinear regime with consideration of mean flow effects and wave–mean flow interaction now needing to be taken into account. The problem presented here is idealized but has general application in the understanding of eddy–eddy and eddy–mean flow interactions as the contrasting limit to that of spatially broad (basinwide) forcing and is relevant given that many sources of oceanic eddies are localized in space.

1. Introduction

The effect of transient eddies on the time-mean state is a fundamental problem in the theoretical studies of the circulation of the atmosphere and ocean. By redistributing momentum, heat, and vorticity in a systematic fashion, eddy flux divergences are capable of having an important impact on the large-scale, time-mean circulation. One way eddies can affect the larger-scale circulation is through the driving of mean motions. Here, we examine this phenomenon through a study of nonlinear rectification, the generation of nonzero mean flow from a forcing with zero mean, in an idealized setup. Specifically, we examine the time-mean flow response of a barotropic and equivalently barotropic fluid subject to a simple eddy vorticity forcing that is localized in space and oscillatory in time. The emergence of the mean flow is a result of nonlinear terms producing finite time-mean fluxes (Reynolds stresses) of momentum and vorticity, whose convergences and divergences act as a driving force for the time-mean flow.

Interest in the problem was originally motivated by its relevance to the dynamics of deep recirculation gyres observed with the eastward jet extensions of western boundary current (WBC) systems such as the Gulf Stream and Kuroshio (Fig. 1). One hypothesis for the driving of these abyssal recirculations originating in historic eddy-resolving ocean circulation studies (see, e.g., Holland and Rhines 1980) is through the action of energetic surface eddies in the thermocline, which act to provide localized sources and sinks of vorticity (''plungers'') to the deep ocean through fluctuating thickness fluxes. Understanding the details of the idealized rectification problem considered here

* Current affiliation: National Oceanography Centre, Southampton, and Grantham Institute for Climate Change, Imperial College, London, United Kingdom.

Corresponding author address: Stephanie Waterman, National Oceanography Centre, Southampton SO14 3ZH, United Kingdom. E-mail: snw@alum.mit.edu

DOI: 10.1175/JPO-D-11-060.1

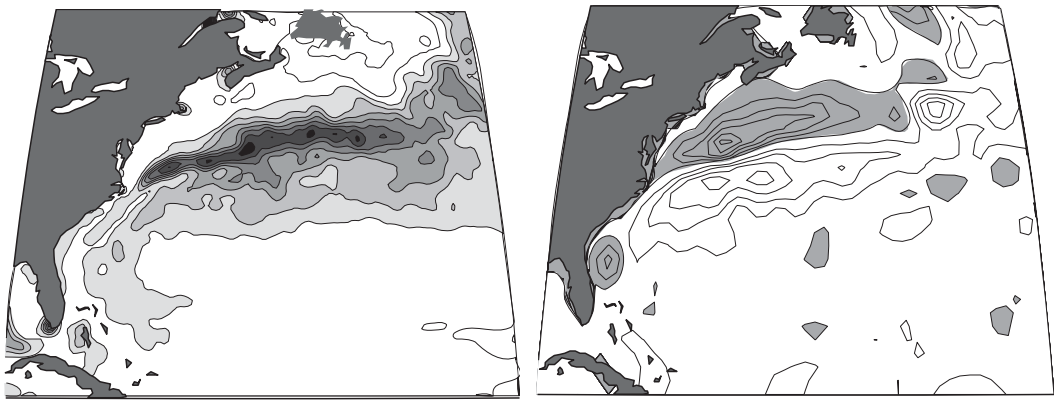

FIG. 1. (left) Time-mean sea surface height variance measured by satellite altimetry 1992–2006 [from Archiving, Validation, and Interpretation of Satellite Oceanographic data (AVISO)] showing a localized concentration of eddy energy along the axis of the Gulf Stream. Contours are in the range of 0.1–0.4 m^2 in intervals of 0.05 m^2. (right) The time-mean dynamic pressure field at 1000-m depth measured by subsurface floats (from Jayne 2006) showing the pair of counterrotating deep recirculation gyres that exist below the jet. Contours are in the range of −0.2 to +0.2 Pa with a contour interval of 0.02 Pa. Negative values are shaded gray.

will aid in evaluating the relevance of this mechanism to driving the deep recirculation gyres (Hogg 1992; Bower and Hogg 1996; Chen et al. 2007; Jayne et al. 2009).

The problem has more general application in our understanding of wave/eddy rectification from a localized forcing, serving as the contrasting limit to spatially broad (basin scale) forcing (Pedlosky 1965; Veronis 1966), and is important, given that many sources of ocean eddies are intermittent in space. For example, rectification from a localized forcing has relevance to the response of the ocean to a spatially localized wind stress pattern or a spatially localized concentration of eddy activity generated by mean flow instability. The radiation of Rossby waves by WBC jets and/or their recirculations (Flierl et al. 1987; Malanotte-Rizzoli et al. 1987; Hogg 1985) make these jet systems themselves potential localized wave sources.

Even more generally, the generation of mean zonal motion by the action of locally forced eddies has relation to the phenomenon of zonal jet formation, observed to occur spontaneously in turbulent β-plane flows (Rhines 1975, 1977; Williams 1979). This process of jet formation by the nonuniform stirring of potential vorticity (PV) resulting in an inhomogeneous distribution of PV gradients (the ''PV staircase'') has been extensively discussed in the literature (Marcus 1993; Vallis 2006; Dritschel and McIntyre 2008). The topic has recently received renewed interest given the discovery of zonal jets in ocean observations (Maximenko et al. 2005) and ocean general circulation models (Nakano and Hasumi 2005; Richards et al. 2006). As discussed in Huang et al. (2007), a deeper understanding of the behavior of the zonal anisotropy in the mean velocities in these studies requires detailed studies based on the dynamical properties of the oceanic eddies/waves and jets, and investigating the scenario that zonal anisotropy is a result of the nonisotropic dispersion relation of Rossby waves may be fruitful.

The work presented here extends earlier studies of eddy-driven mean flow from localized forcing, specifically the pioneering laboratory experiments by Whitehead (1975) and numerical simulations by Haidvogel and Rhines (1983, hereafter HR83). The former was the first experimental demonstration of the generation of mean zonal currents from a localized periodic forcing, whereas the latter examined this phenomenon numerically through simulations of two-dimensional flow on a midlatitude β plane. In their analysis, HR83 make many insights into the rectification mechanism that forms the starting point for the present study. Notably they demonstrate the usefulness of the analytical solution in the form of a time-periodic Green's function in understanding the forced wave field. Furthermore, from analysis of their numerical simulations, they demonstrate that the dynamics of the rectified circulation is related to the mean meridional eddy PV flux and that regions of counter (up) gradient PV fluxes provide the propulsion necessary for fluid particles to cross the mean quasigeostrophic contours.

The present work seeks to extend HR83 in several ways. Specifically the work presented here aims to

(i) examine the rectification mechanism in more detail through examination of the eddy flux convergences of momentum and vorticity and the eddy enstrophy balance;
(ii) extend the study of parameter variations of the forcing and the flow and understand the mean flow dependence on these parameters in terms of the dynamics of the rectification mechanism;

(iii) explore and understand the effects of stratification;
(iv) explore and understand the effects of a background mean flow; and
(v) extend these results from the weakly nonlinear to the fully nonlinear regime to examine which results from the small forcing amplitude limit breakdown.

Finally, we seek to comment on the potential relevance of the mechanism in driving mean flows in the oceanic context.

This paper is organized as follows: In section 2, we describe insights into the rectification mechanism gained from an analytical expansion solution that is valid in the weakly nonlinear limit. In section 3, we describe numerical simulations and insights gained from the examination of the nonlinear eddy–mean flow interaction. In section 4, we discuss the results of numerical model parameter studies, describing the dependence of the strength of the rectified flow generated for various forcing and flow parameters, stratification, and mean background flows. In section 5, we extend our study from a weakly nonlinear regime to a strongly nonlinear regime. In the final section, we discuss the relevance of the study to oceanic applications.

2. Analytical solution

Following HR83, we consider the problem in the context of the quasigeostrophic potential vorticity (QGPV) equation on a midlatitude β plane forced by a spatially localized, oscillatory vorticity source. We add the effect of stratification by considering the dynamics in a reduced gravity configuration. This setup is an idealized model for motion in the deep ocean forced by a fluctuating thermocline above and is relevant to the driving of the deep recirculation gyres in WBC jet systems. The governing equation expressing the conservation of QGPV that we consider is

$$\frac{\partial}{\partial t}q + J(\psi, q) = AF(x,y)\cos(\omega t) - r_{\text{spin}}\zeta, \qquad (1)$$

where q, the QGPV, is given by $q = \nabla^2\psi - (1/R_D^2)\psi + \beta y$. Here, x is the zonal coordinate, y is the meridional coordinate, and t is time. The variable ψ is the streamfunction such that the horizontal velocity components are given by $u = -(\partial/\partial y)\psi$ and $v = (\partial/\partial x)\psi$, and $\zeta = \nabla^2\psi$ is the relative vorticity. Here, r_{spin} is the barotropic spindown rate, the inverse time scale for vorticity decay due to linear (bottom) friction. We choose linear friction as our parameterization of dissipative effects here but note that numerical simulations with Laplacian (lateral) viscosity give qualitatively similar results in the weakly dissipative regime we consider. The variable R_D is the Rossby deformation radius, and β is the meridional gradient of planetary vorticity. The forcing $AF(x, y)\cos(\omega t)$ is of the form of a localized oscillatory source/sink of vorticity (with zero time-mean vorticity input) fixed at the center of the basin with amplitude A, an angular frequency ω, and a spatial distribution described by $F(x, y)$. It can be interpreted as a localized and time-varying vertical velocity of the form $(f_0/D)w(x, y, t)$, where f_0 is the reference Coriolis frequency, D is the barotropic ocean depth, and w is the vertical velocity at a layer interface.

We nondimensionalize (1) in terms of dimensionless variables $\hat{x}, \hat{t}$, and $\hat{\psi}$ and dimensional scales L, T, and U. We scale length and time by the external forcing parameters (taking L to be the characteristic length scale of the forcing and T to be the inverse of the forcing frequency) and scale U assuming a dominant balance of relative vorticity spinup and forcing (the expected high-frequency balance for Rossby waves) such that $U = AL/\omega$. The scaled governing equation can then be written in the form

$$\frac{\partial}{\partial \hat{t}}\hat{\nabla}^2\hat{\psi} - S^{-1}\frac{\partial}{\partial \hat{t}}\hat{\psi} + \mu\hat{J}(\hat{\psi}, \hat{\nabla}^2\hat{\psi}) + \beta^*\frac{\partial}{\partial \hat{x}}\hat{\psi} = F(\hat{x}, \hat{y})\cos(\hat{t}) - R\hat{\nabla}^2\hat{\psi}. \qquad (2)$$

Equation (2) shows the dependence on the nondimensional parameters governing the problem: $S^{-1} = L^2/R_D^2$ is the inverse Burger number and is a measure of stratification; $\beta^* = \beta L/\omega$ is the nondimensional planetary vorticity gradient and represents the relative importance of the planetary vorticity gradient to the gradients of relative vorticity; and $\mu = U/\omega L = A/\omega^2$ is the wave steepness and gives the degree of nonlinearity of the waves. Finally, $R = r_{\text{spin}}T$ is the nondimensional linear friction coefficient, which is the inverse of the spindown time relative to the characteristic time scale.

To gain insight into the rectification mechanism and the relation between the forcing parameters and the rectified flow, we appeal to an analytical description of the forced waves. As in HR83, we exploit the Green's function solution to the governing equation (2) in the absence of friction, extending their analysis to include a dependence on the inverse Burger number. This simplification of (2), after dropping the hats for notational simplicity, is

$$\frac{\partial}{\partial t}\nabla^2\psi - S^{-1}\frac{\partial}{\partial t}\psi + \mu J(\psi, \nabla^2\psi) + \beta^*\frac{\partial}{\partial x}\psi = \delta(\mathbf{x})e^{-it}. \qquad (3)$$

Equation (3) cannot be solved in closed form because of the nonlinear self-advection of relative vorticity, $J(\psi, \nabla^2\psi)$. If the forcing amplitude is small, however, one can

make progress by expanding the solution in powers of the forcing amplitude. We set the nondimensional forcing amplitude such that μ is a small parameter. We then take ψ to have the form

$$\psi = \mu\psi_1 + \mu^2\psi_2 + \cdots \tag{4}$$

Substituting (4) into (3) and equating terms of the same order of μ then yields

$$\text{order } \mu\text{: } \frac{\partial\nabla^2\psi_1}{\partial t} - S^{-1}\frac{\partial}{\partial t}\psi_1 + \beta^*\frac{\partial\psi_1}{\partial x} = \delta(\mathbf{x})e^{-it} \quad \text{and} \tag{5}$$

$$\text{order } \mu^2\text{: } \frac{\partial\nabla^2\psi_2}{\partial t} - S^{-1}\frac{\partial}{\partial t}\psi_2 + J(\psi_1, \nabla^2\psi_1) + \beta^*\frac{\partial\psi_2}{\partial x} = 0. \tag{6}$$

The order μ equation is a linear equation whose solution is

$$\psi_1(x, y, t) = H_o^{(2)}(\gamma r)e^{-i(Bx+t+\pi/2)}, \tag{7}$$

where $H_o^{(2)}$ is the Hankel function of the second kind, $\gamma^2 = B^2 - S^{-1}$ is the radius of the Rossby wave dispersion circle, $B = \beta/2\omega$ is the radius of the barotropic Rossby wave dispersion circle, and $r = \sqrt{x^2 + y^2}$ is the radius from the origin of the forcing. This solution has the same form as the barotropic problem described by HR83, but with γ replacing B in the argument of the Hankel function. [We also note that we have corrected the sign error for the time-dependent term and the phase shift factor in the argument of the exponential to Eq. (3.2) of HR83.]

This more generalized solution immediately shows two important effects of stratification on the problem. First, stratification reduces the wavenumber of the response shifting the excited wave field to longer wavelengths than in the absence of stratification. Second, it introduces a new cutoff, as for sufficiently large values of the inverse Burger number (such that γ becomes imaginary) radiating solutions no longer exist. The appreciation of these effects aids in the interpretation of the results of the numerical parameter study varying stratification discussed in section 4.

The first contribution to the time-mean flow enters at order μ^2. Taking the time mean of (6) yields

$$\overline{J(\psi_1, \nabla^2\psi_1)} + \beta^*\frac{\partial\overline{\psi}_2}{\partial x} = 0. \tag{8}$$

Rearranging to solve for $\overline{\psi_2}$, the time-mean streamfunction associated with the rectified flow, then gives

$$\overline{\psi}_2 = -\frac{1}{\beta^*}\int_x^{x_E}\overline{J(\psi_1, \nabla^2\psi_1)}\,dx. \tag{9}$$

The second-order time-mean flow is given by the zonal integral (to the eastern boundary x_E) of the time-mean eddy relative vorticity flux divergence of the first-order, linear forced wave field. It is important to note the first-order field has a zero time mean.

The first-order wave field, its time-mean eddy vorticity flux divergence, and the second-order time-mean flow it drives for the Green's function solution (7) in the barotropic limit are shown in Fig. 2 (top). The Green's function solution does not produce a time-mean rectified flow outside the immediate vicinity of the forcing, a consequence of the east–west antisymmetric pattern of vorticity flux divergence that, because of its exact zonal antisymmetry and the dependence of the rectified flow on the zonal integral of the flux divergence, produces zero rectified flow in the far field.

Hypothesizing that a finite forcing extent may be critical to producing rectified flow, we introduce spatial dependence to the forcing function and compute the particular solution for a forcing dependence $F(\mathbf{x})$ by numerically evaluating the convolution integral

$$\psi_{1P} = \int\psi_1(\mathbf{x}, \mathbf{x}')F(\mathbf{x}')\,d\mathbf{x}'. \tag{10}$$

Various forms of the function $F(x, y)$ were considered; however, for the mechanism that we describe here, it is important only that the forcing be sufficiently localized in space (sufficiently localized will be discussed later). To supply a localized forcing and yet still allow a large range of amplitudes to be considered, we favor a forcing function of the form

$$F(\mathbf{x}) = F(r) = \left(1 - \frac{r^2}{L_F^2}\right)e^{-(r/L_F)^2}, \tag{11}$$

where r is the radius from the origin of the forcing and L_F is the forcing length scale. With this particular forcing, at any instant in time the basin integral of the PV input due to the forcing is approximately zero (it is exactly zero for infinite basin size), whereas the PV forcing input is concentrated within a radius L_F of the plunger's center. Note, however, that the results described remain robust for the forcing used by HR83.

As before, to compute the time-mean rectified flow associated with this wave field, we compute the zonal integral of the time-mean Jacobian using the particular solution ψ_{1P} in place of ψ_1. We show the wave field, its time-mean eddy vorticity flux divergence, and the time-mean flow that it drives in Fig. 2 (bottom). In contrast to

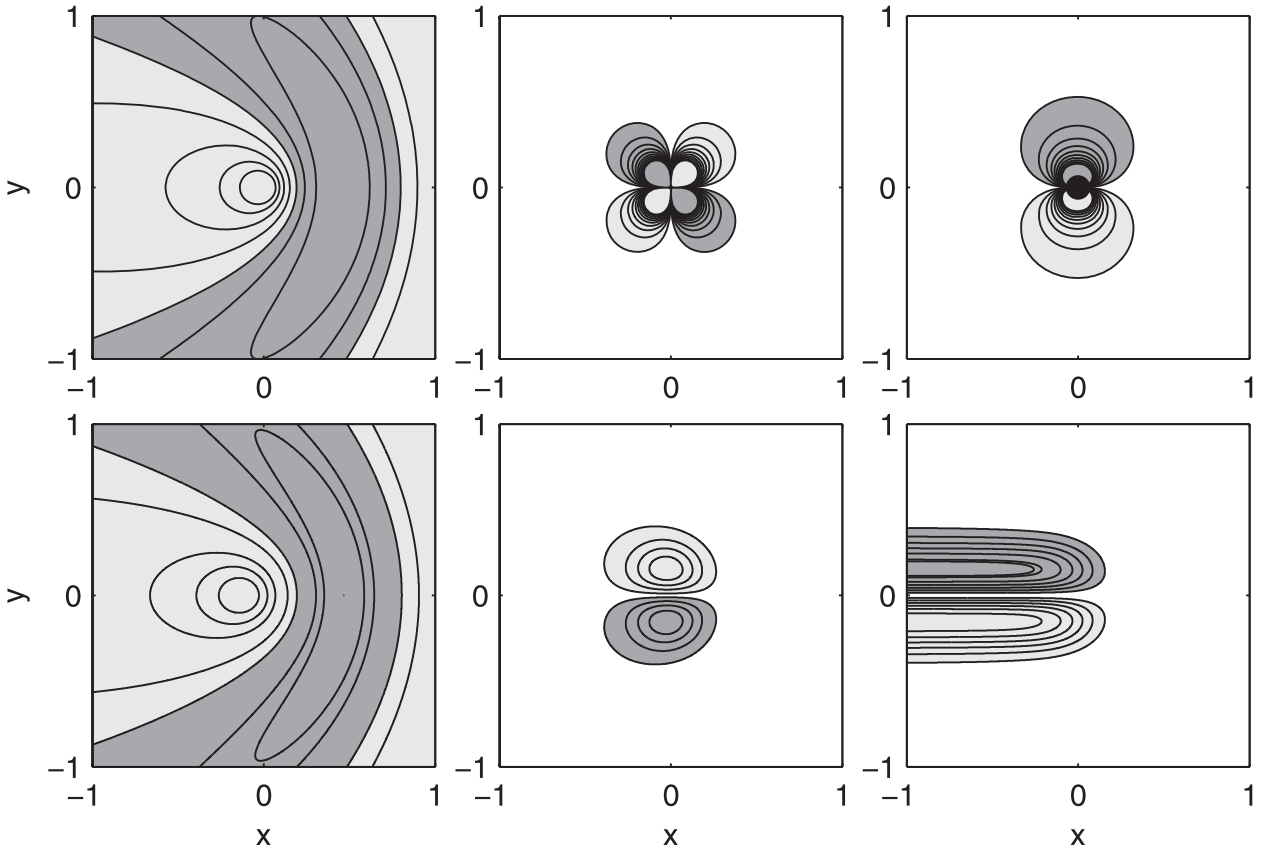

FIG. 2. A comparison of properties of the analytical solutions for (top) a forcing function with a delta function spatial dependence (the Green's function solution) ($\beta^* = 0.05$) versus (bottom) a forcing function with a Laplacian of a Gaussian spatial dependence ($\beta^* = 0.05$, $\mu = 0.25$, and $L_F = 0.1$): (left) the wave field (as visualized by a snapshot of the instantaneous streamfunction), (middle) the time-mean eddy vorticity flux divergence that drives the time-mean rectified flow, and (right) the resulting time-mean rectified flow (as visualized by the time-mean streamfunction). Positive values are shaded light gray, and negative values are shaded dark gray (here and in all following contour plots).

the Green's function solution, the particular solution for a forcing function with finite spatial extent does produce a pattern of vorticity flux divergence whose zonal integral is consistent with the two-gyre circulation pattern with an eastward jet at the latitude of the forcing and westward flow north and south of this. We conclude that, at least in the weakly nonlinear, inviscid limit, it is necessary for the forcing to have a finite length scale in order to generate rectified flow in the far field. The contrast between the solutions also implies that the mechanism that is generating the rectified flow is occurring inside the forcing region (where the Green's function and particular solution differ) and not by the waves in the far field (where they do not).

3. Numerical simulations

To examine the effect of the full nonlinearities on the problem, we perform numerical simulations of the solution to (2) with the forcing specified by (11). We use the simulations to diagnose the nonlinear terms responsible for the driving of the time-mean flow and explore the dependence of the rectification mechanism on flow and forcing parameters. Integration in time and space is done using a scheme that is center differenced in the two spatial dimensions (an ''Arakawa A grid'') and stepped forward in time using a third-order Adams–Bashforth scheme (Durran 1991). Advective terms are handled using the vorticity-conserving scheme of Arakawa (1966). Further details on the numerical method can be found in Jayne and Hogg (1999). The nondimensional grid spacing is 0.1 nondimensional length units and the number of grid points is 6001 (east–west) $\times$ 6001 (north–south). With the origin at the center of the domain, this puts the western boundary at $x = -300$ and the northern boundary at $y = 300$ nondimensional length units. The domain is closed with solid wall boundaries, and dissipative sponge layers, 2000 grid points wide, are placed next to all boundaries to absorb all waves leaving the domain. The width of these sponge layers is chosen to be sufficient to eliminate basin

modes from the domain. In the interior, we examine the solution in the limit where the nondimensional linear friction coefficient R is small enough that dissipation is negligible in the time-mean vorticity balance. This near-inviscid limit is of interest both because it allows us to apply the theoretical considerations derived by HR83, and because, by minimizing the effect of friction, the dominant balances are simplified and emphasize eddy effects. In the ''typical run'' simulation (which we describe here in detail and around which parameter studies are varied), we set $S^{-1} \to 0$ (the barotropic rigid-lid limit), $\mu = 0.25$, $\beta^* = 0.05$, and $R = 5 \times 10^{-8}$. These choices are consistent with, for example, dimensional scales L and T representing forcing length and time scales of $L_F = 250$ km and $\omega = 2\pi/60$ days^{-1}. They imply a forcing amplitude equivalent to a peak vertical velocity of $\sim 2 \times 10^{-5}$ m s^{-1} (here we assume a midlatitude value of $\beta = 2 \times 10^{-11}$ m^{-1} s^{-1}, a midlatitude value of $f = 1 \times 10^{-4}$ s^{-1}, and a barotropic ocean depth of $D = 5000$ m) and an inverse barotropic spindown time in the interior of $\sim$(1/30 000) yr^{-1}. As such, the forcing scales and nondimensional parameters are typical of oceanic synoptic scales in a midlatitude ocean. The very weak interior friction implies that a rectified flow would extend west to nearly infinity were it not for the western sponge layer, which closes the recirculations before the expected distance $\beta L^2/R$ (the distance traveled by a wave with speed βL^2 in a spindown time of $1/R$) (Rhines 1983; Hsu and Plumb 2000).

The Reynolds stresses of vorticity diagnosed in the numerical simulations (shown for the typical set of parameters in Fig. 3) illustrate that the key to the eddy generation of mean flows is a systematic up-gradient (northward) eddy flux of potential vorticity that occurs in the vicinity of the forcing. This eddy transport produces a flux convergence in the northern half and a flux divergence in the southern half of the forced region. Based on the notion that the time-mean eddy flux divergence drives the mean rectified flow through the relation $\overline{\psi} = -1/\beta^* \int \overline{J(\psi', \nabla^2\psi')}\, dx$ (valid in the weakly nonlinear limit), it is responsible for the driving of the time-mean recirculation gyres that extend outside the vicinity of the forcing. This up-gradient flux of PV in the forced region is inevitable in view of the overall zonal momentum balance: stirring of the background PV at latitudes free of forcing drives westward mean momentum at those latitudes, and, if the forcing is specified to exert no mean zonal force as is the case here, then the zonal momentum integrated over the entire domain must go to zero. Hence an upgradient PV flux and the driving of eastward zonal mean momentum at the forced latitudes is required (Rhines 1977, 1979). Given this picture, we hypothesize that the properties of the mean flow generated will be closely related to the process of up-gradient eddy vorticity transport in the vicinity of the plunger.

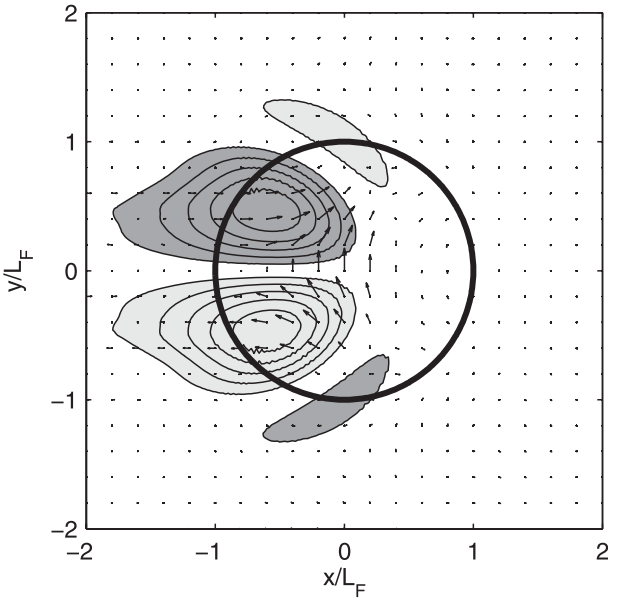

FIG. 3. Eddy vorticity transport ($\overline{u'q'}\mathbf{i} + \overline{v'q'}\mathbf{j}$) (vectors) overlaid on the eddy vorticity transport divergence [$\overline{J(\psi', q')}$] (contours) for the typical run parameters ($S^{-1} \to 0$, $\mu = 0.25$, $\beta^* = 0.05$, and $R = 5 \times 10^{-8}$).

Further insight comes from consideration of the eddy enstrophy budget. The eddy PV flux across time-mean contours of PV features in the steady-state eddy enstrophy equation, which can be rearranged to express the eddy vorticity flux relative to the mean PV gradient, $\overline{\mathbf{u}'q'} \cdot \nabla\overline{q}$, as the sum of the other terms in the enstrophy budget: enstrophy injection by the forcing, dissipation, and the advection of eddy enstrophy by the mean flow and the self-advection of eddy enstrophy, respectively (Rhines and Holland 1979). Visualization of the various terms in the enstrophy budget in the numerical simulation output reveals that, for the typical set of parameters, an up-gradient eddy vorticity flux inside the forcing region (Fig. 4, left) is predominantly balanced by the enstrophy injection supplied by the forcing (Fig. 4, right). As such, the up-gradient eddy fluxes responsible for driving the mean flows are permitted because enstrophy injection supplied by the forcing dominates over all other sources and sinks of enstrophy in the time-mean budget in the near field of the forcing. This suggests that the rectification mechanism will remain robust as long as this time-mean enstrophy balance is maintained, and it also highlights the importance of the term $\overline{F_q'q'}$ expressing the time-mean correlation between the fluctuating potential vorticity input supplied by the forcing F_q' and the perturbation vorticity in the fluid that

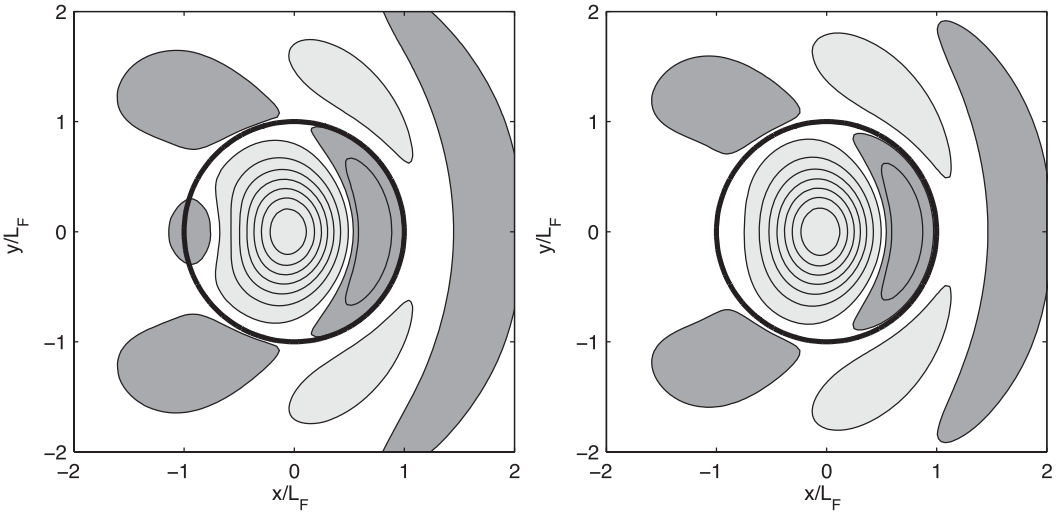

FIG. 4. (left) The eddy vorticity flux relative to the time-mean PV gradient ($\overline{\mathbf{u}'q'} \cdot \nabla\overline{q}$) and (right) the time-mean injection/removal of enstrophy by the forcing ($\overline{F_q'q'}$). Parameters are as in Fig. 3.

is generated in response q' being positive. The importance of this positive correlation provides insight into why localized forcing is effective at producing rectification: a forcing scale smaller than the wavelength of the fluid response guarantees $\overline{F_q'q'}$ to be single signed and positive everywhere inside the forced region. It also demonstrates the importance of the forcing region, where $\overline{F_q'q'}$ is nonzero.

Finally, Reynolds stresses of zonal momentum and their divergence (Fig. 5) provide further insight. In this framework, the mean zonal flows are driven by eddy "forces" that arise from a systematic eddy flux of zonal momentum toward the forcing region. This pattern of eddy zonal momentum flux is a result of the outward energy radiation of the Rossby waves emanating from the forcing, as first discussed by Thompson (1971), producing an eddy zonal momentum flux convergence in the forced zone and eddy zonal momentum flux divergences northwest and southwest of the forcing. Interpreting this eddy flux divergence quantity as a parameterization of an effective steady zonal eddy force, this pattern then translates to a positive (eastward) eddy force at the latitude of the forcing and negative (westward) eddy forces north and south of the forcing. In this way, eddies act to accelerate the eastward jet at the forced latitudes and drive the flanking westward flows. We note that the interpretation of the eddy effect on the time-mean flow in terms of momentum must be done with caution, because, in a nonzonally averaged time-mean framework, the Reynolds stress divergence of zonal momentum can act to accelerate zonal flows or balance the Coriolis torque of the time-mean residual (in this case ageostrophic) circulation. In addition, eddy momentum fluxes can be contaminated by a large rotational component that is balanced in the momentum budget by the time-mean pressure gradient and does not act to accelerate time-mean flows. Full treatment should consider a generalization of the Eliassen–Palm (E–P) flux appropriate for time-mean flows such as the E-vector approach of Hoskins et al. (1983), the radiative wave activity flux described by Plumb (1985, 1986), or the localized E-P flux developed by Trenberth

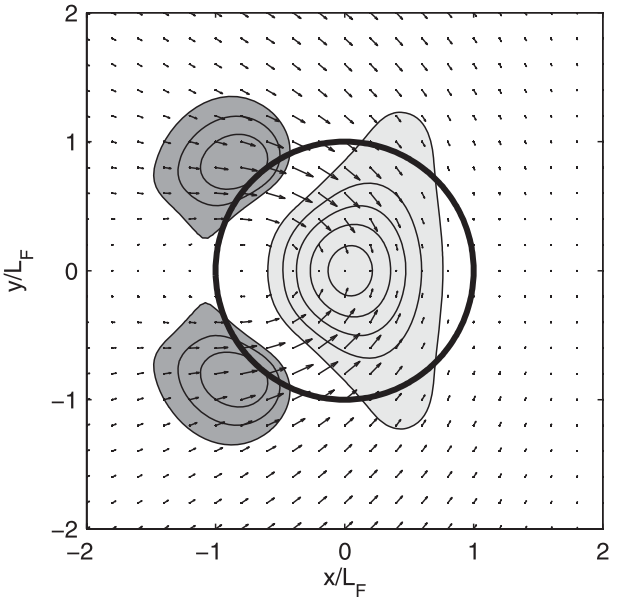

FIG. 5. Eddy zonal momentum transport ($\overline{u'u'}\mathbf{i} + \overline{u'v'}\mathbf{j}$) (vectors) overlaid on the eddy zonal momentum transport convergence $\{-[(\partial/\partial x)\overline{u'u'} + (\partial/\partial y)\overline{u'v'}]\}$ (contours) for the typical run parameters as in Fig. 3.

TABLE 1. Summary of numerical experiments. Here, U_o is the magnitude of a dimensionless constant background flow described in section 4.

Nondimensional parameter	Range of values	Dimensional variable	Range of scales
S^{-1}	0–0.3	R_D	∞–100 km
μ	0.25–4.0	w_{Ek}	2×10^{-5}–3×10^{-4} m s^{-1}
β^*	0.01–0.15	B^{-1}	4000–250 km
R	5×10^{-8}–1×10^{-2}	r_{spin}	(1/30 000)–(1/0.1) yr^{-1}
U_o^*	−0.1 to +0.1	U_o	−1 to 1 cm s^{-1}
		L_F	50–750 km

(1986). In this case, however, the key features of a convergence of eastward momentum flux at the forcing latitudes and of westward momentum flux north and south of the forcing remain key features of the eddy zonal momentum forcing in these other more complete diagnostics. As such, there is heuristic value in the consideration of the eddy zonal momentum fluxes alongside the eddy vorticity fluxes (which are dependent only on the relevant divergent component of the eddy flux), because they provide additional insight into the rectification mechanism: namely connecting rectification to the process of wave energy radiation from the forcing. We hypothesize as a result that the properties of the eddy-driven mean flow will be closely tied to the properties of wave energy radiation.

4. Dependence on system parameters

a. The effect of forcing and flow parameters

In a suite of simulations, we vary the nondimensional β parameter and the dimensional forcing radius to explore how each affects the strength of the rectified flow (see Table 1 for a summary of the parameter ranges). The strength of the mean flow generated (the ''rectification strength,'' which we define as the maximum time-mean gyre transport, $\overline{\psi}_{\max} - \overline{\psi}_{\min}$) has a nonmonotonic dependence on these parameters (Fig. 6), a behavior that highlights the importance of the character of the Rossby waves excited by the forcing in setting the rectification response. One can understand why this is the case based on the understanding of the rectification mechanism outlined in the previous section. In short, varying which waves (i.e., the pairs of wavenumbers k and l) that are preferentially excited by the forcing in the spectrum of free Rossby waves available (a function of the forcing spectrum and hence of L_F and of the dispersion relation, $\omega = -\beta k/(k^2 + l^2)$, and hence of β and ω, respectively) changes the properties of wave energy radiation away from the forcing through the dependence of the waves' group velocity on wavenumber. This dictates the spatial distribution of wave activity, which in turn changes the rectified flow response because rectification depends directly on the spatial gradients of the wave/eddy terms. We find a resonant-like maximum response occurs when the length scale of the forcing is well matched to the spectrum of free Rossby waves available, in particular when L_F is close to $1/B$ (Fig. 6). The length scale $L_F = 1/B$ is the most effective forcing scale for producing rectified flow because it preferentially excites the wave in the available Rossby wave spectrum with zero zonal group velocity and maximized meridional group velocity and as such is optimal for exciting waves that radiate meridionally.

An illustration of how the selection of excited wavenumbers by the forcing length scale impacts rectification efficiency is shown in Figs. 7 and 8. We illustrate the

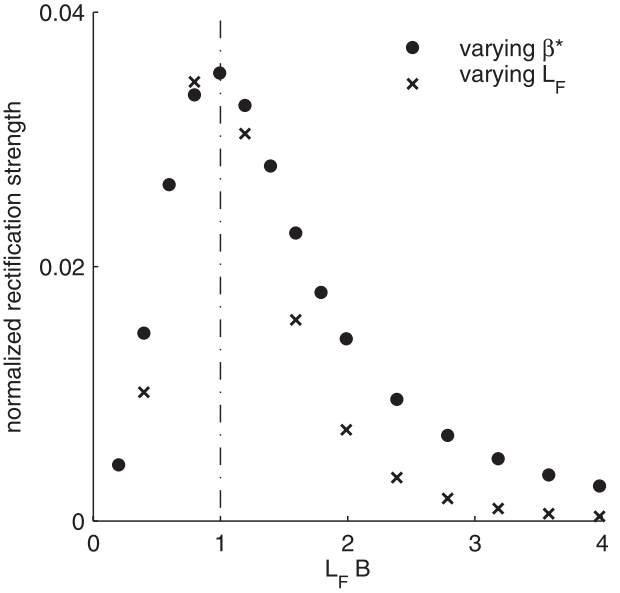

FIG. 6. Dependence of the rectification strength ($\overline{\psi}_{\max} - \overline{\psi}_{\min}$) on the nondimensional β^* parameter (circles) and the forcing radius L_F ($\times$ symbol). If not being varied, parameters are fixed at the typical run values of $\beta^* = 0.05$ and $L_F = 250$ km. In all cases, $S^{-1} = 0$. Rectification strength is normalized by the PV input supplied by the forcing in one-half period to make the ratio of the response to forcing strength equivalent for each set of runs. A resonant response occurs when the forcing length scale L_F is equal to $1/B$.

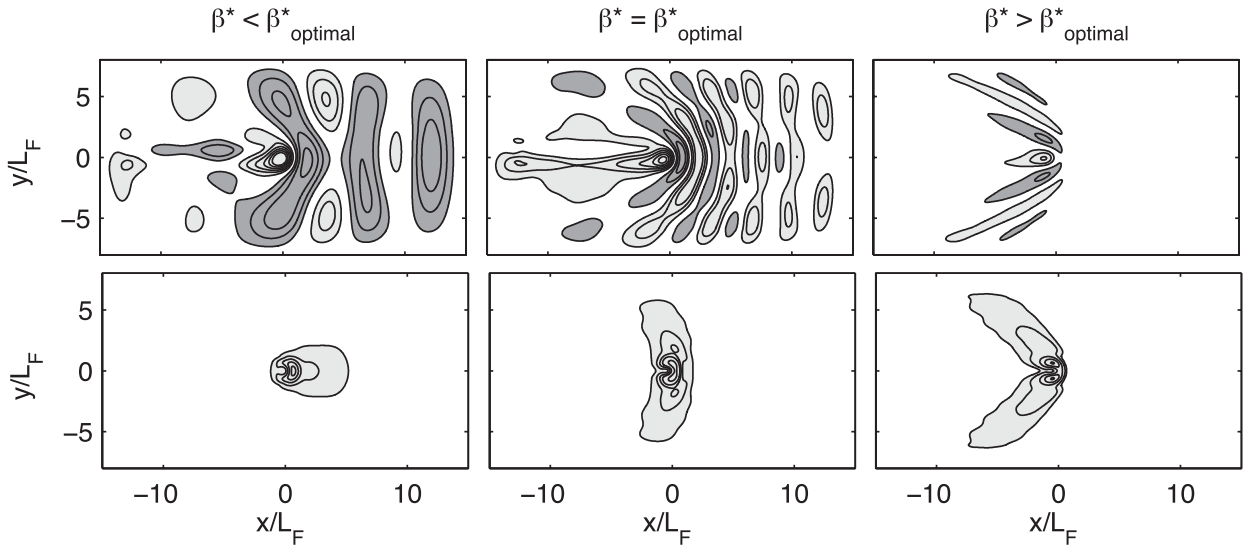

FIG. 7. The effect of varying β^* from $\beta^* < \beta^*_{\text{optimal}}$ to $\beta^* > \beta^*_{\text{optimal}}$ on (top) the waves excited (as visualized by a snapshot of the instantaneous streamfunction) and (bottom) the orientation of energy radiation from the forcing (as visualized by the time-mean eddy kinetic energy). Values of β^* corresponding to suboptimal, optimal, and superoptimal are 0.015, 0.025, and 0.035, respectively.

excited wave field, the time-mean eddy kinetic energy distribution, and the eddy forcing terms for a fixed size plunger and three representative values of β^*: one such that $L_F = 1/B\,(\beta^*_{\text{optimal}})$, one with $\beta^* < \beta^*_{\text{optimal}}$ $(L_F < 1/B)$, and one with $\beta^* > \beta^*_{\text{optimal}}$ $(L_F > 1/B)$ (see Fig. 9). The effect of changing β^* changes the character of the waves that are excited by the forcing consistent with expectations based on the intersection of the inverse forcing length scale $1/L_F$ and the dispersion circle: for $\beta^* < \beta^*_{\text{optimal}}$ the wave field is dominated by waves with

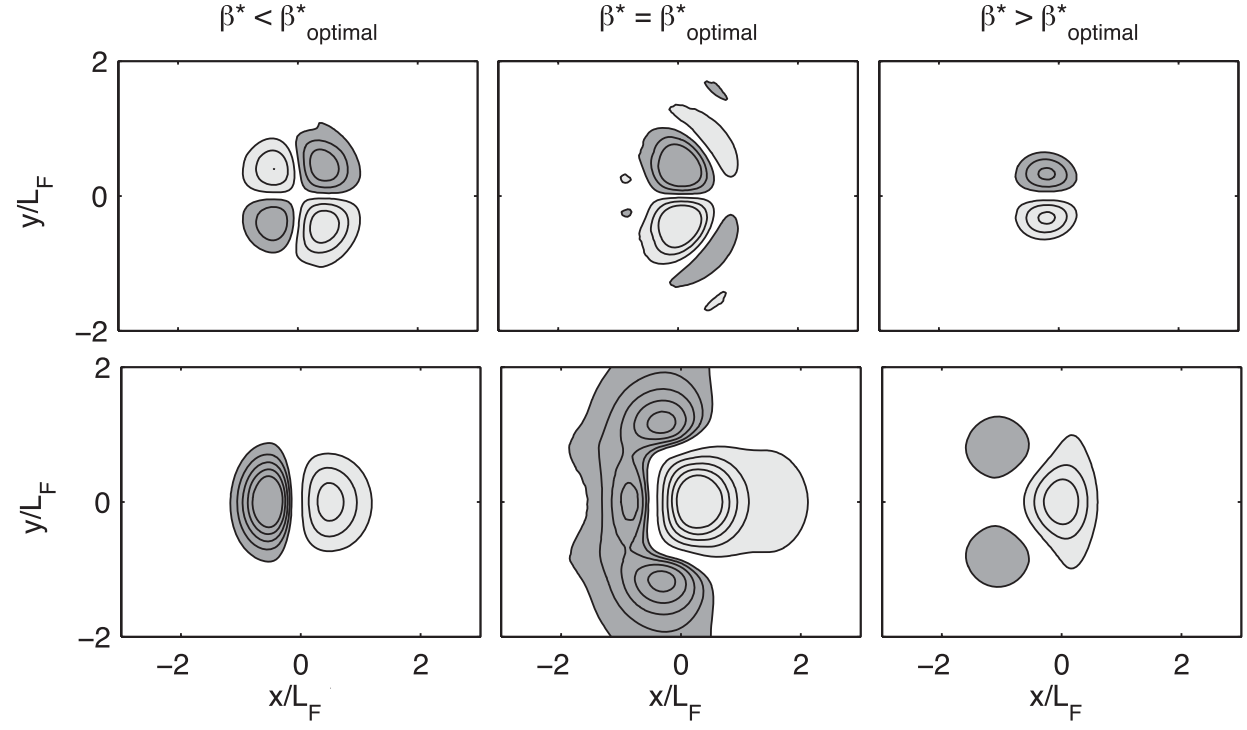

FIG. 8. The effect of varying β^* from $\beta^* < \beta^*_{\text{optimal}}$ to $\beta^* > \beta^*_{\text{optimal}}$ on (top) the patterns of eddy vorticity flux divergence and (bottom) the patterns of eddy zonal momentum flux convergence. Values of β^* corresponding to suboptimal, optimal, and superoptimal are as in Fig. 7.

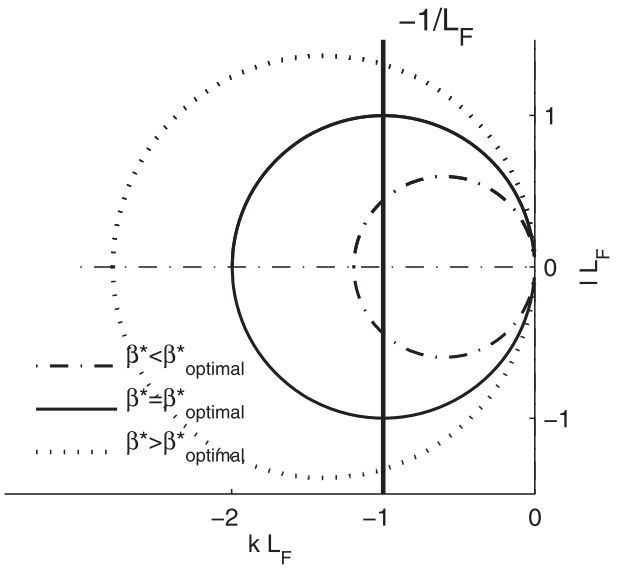

FIG. 9. A visualization of the relation between the forcing length scale L_F and the Rossby wave dispersion relation for fixed frequency for the three values of β^* discussed in the text. Here, values of β^* of 0.015, 0.025, and 0.05 are visualized as the suboptimal, optimal, and superoptimal β^* values, respectively.

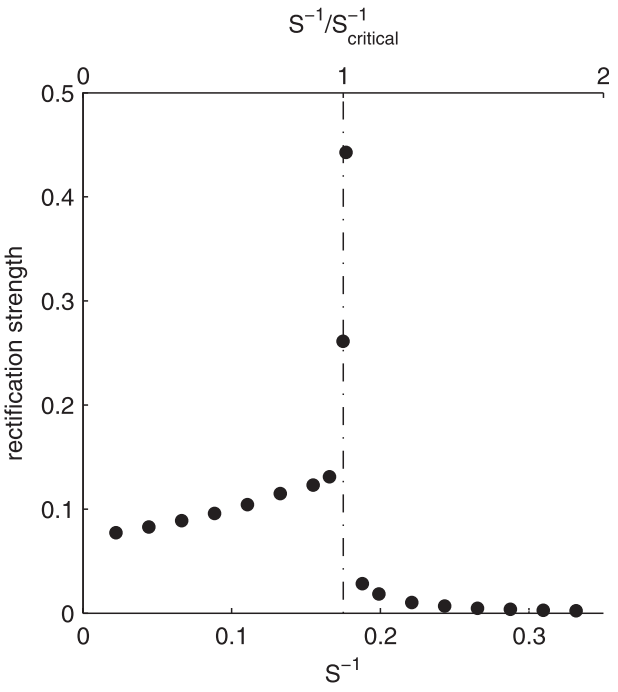

FIG. 10. Dependence of rectification strength on the inverse Burger number S^{-1}. The dependence on S^{-1} normalized by $S^{-1}_{\text{critical}} = B^2$, that is, the inverse Burger number that makes the radius of the dispersion circle zero and beyond which the analytical solution predicts radiating solutions cease to exist, is shown on the upper axis.

large meridional scale relative to their zonal scale ($|k| > |l|$), whereas for $\beta^* > \beta^*_{\text{optimal}}$ the wave field is dominated by waves oriented more zonally ($|k| < |l|$) (Fig. 7, top). This change in the wavenumbers that are excited changes the pattern of the waves' energy radiation through the Rossby waves' group velocity dependence on wavenumber: as β^* is varied from suboptimal to superoptimal, the waves that are excited change from waves with predominantly eastward group velocity to waves that have a predominantly westward zonal group velocity component. Waves with a significant meridional group velocity are included in the excited spectrum when β^* is such to include waves near $(k, l) = (-B, \pm B)$ in the excited range. This impacts the time-mean eddy kinetic energy distributions for the three cases (Fig. 7, bottom). Finally, the changing properties of energy radiation impact rectification strength through changing the spatial distributions of the Reynolds stresses, $\overline{u'u'}$, $\overline{u'v'}$, and $\overline{v'v'}$, spatial gradients of which determine the eddy forcing terms. Both a zonal asymmetry and a significant meridional component of energy radiation are required for effective rectification, requirements that can be understood through consideration of the patterns of eddy vorticity flux divergence and eddy zonal momentum flux divergence, respectively (Fig. 8). Zonal asymmetry in energy radiation results in a significant change in the pattern of the eddy vorticity flux divergence from the zonally antisymmetric four-lobed pattern that results from a zonally symmetric radiation of energy (and generates no mean flow outside the forcing region) to the two-lobed pattern that results from a zonally asymmetric radiation of energy (and drives the counter-rotating gyres west of the forcing region) (Fig. 8, top). A large component of meridional energy radiation separates (in latitude) the regions of eddy momentum flux convergence and divergence to avoid their mutual cancelation in the driving of the mean flow (Fig. 8, bottom).

b. *The effect of stratification*

Numerical parameter studies varying the Burger number reveal that rectification strength has a nonmonotonic dependence on stratification (Fig. 10), and again one can understand the dependence as a result of changes in the waves that are selected to participate in the rectification process. In this 1½-layer configuration, the streamfunction and PV thickness contours are coincident and there is no advection of the stretching component of the PV. As such, rectification continues to result only from the advection of relative vorticity as in the barotropic case. Stratification does alter the barotropic problem, however, by changing the radius of the dispersion circle, and this has two important implications for the characteristics of the waves selected by the forcing. First, by reducing the spectrum of free wavenumbers available, increasing stratification concentrates the forcing

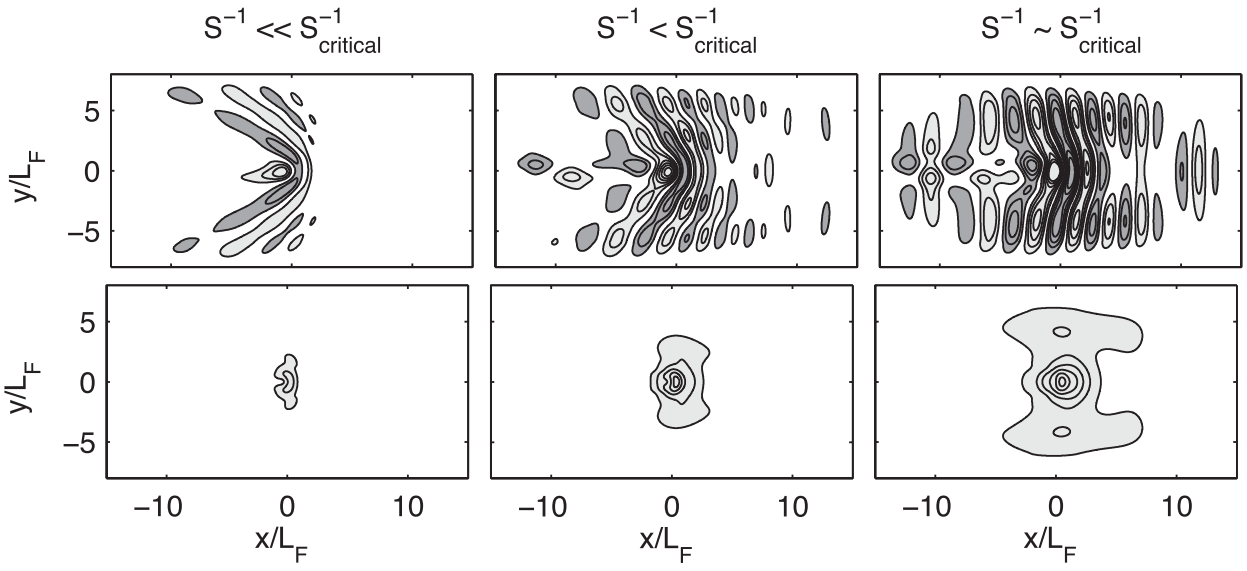

FIG. 11. The effect of varying stratification by increasing S^{-1} toward the critical value on: (top) the waves excited (as visualized by a snapshot of the instantaneous streamfunction) and (bottom) the orientation of energy radiation from the forcing (as visualized by the time-mean eddy kinetic energy). Values of S^{-1} are 0.05, 0.10, and 0.15. Other forcing and flow parameters are set to the typical run values as in Fig. 3.

amplitude into a narrower band of wavenumbers with increased wave amplitudes. Second, increasing stratification centers the excited spectrum more narrowly around $|k| = B$. Snapshots of the excited wave fields and the orientation of their energy radiation for various values of S^{-1} (Fig. 11) illustrate these effects. In this way, a finite deformation radius traps energy near the forcing and amplifies the meridional fluid velocity. The forced flow is more effective at stirring PV and the strength of the rectified flow increases as a result. A singularity arises at the critical value where only the wave $(k, l) = (-B, 0)$ satisfies the dispersion relation, a wave with zero group velocity in both the zonal and meridional directions and as such no propagation of wave energy away from the forcing region. For larger stratifications, the radius of the dispersion circle becomes imaginary. No real pairs of wavenumbers (k, l) satisfy the dispersion relation, and, as suggested by the analytical solution, the forcing fails to radiate waves. The strength of the rectified flow goes to zero as a result.

c. The effect of a mean background flow

We add a large-scale mean background flow to the setup by adding a constant, uniform, zonal background mean flow U_o^* to (2) by modifying the advection term $J(\psi, \nabla^2\psi)$ to include advection also by the background flow $\Psi = -U_o^* y$. We then examine the impact of varying the magnitude and direction of U_o^* in the numerical simulations. The addition of a uniform mean flow puts us into the regime studied by Lighthill (1967), with a moving oscillating forcing function and its important dependence on the sign of U_o.

Results of these parameter studies (Fig. 12) again show a nonmonotonic dependence on U_o, and again the

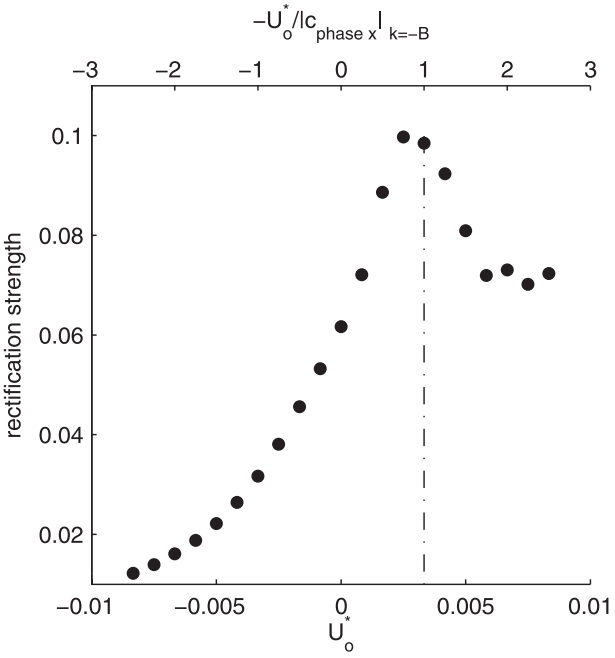

FIG. 12. Dependence of rectification strength on the value of the constant zonal background flow U_o^*. The dependence on $-U_o^*$ normalized by the magnitude of the net zonal phase speed of the wave with the optimal zonal wavenumber $|k| = B$ is shown on the upper axis.

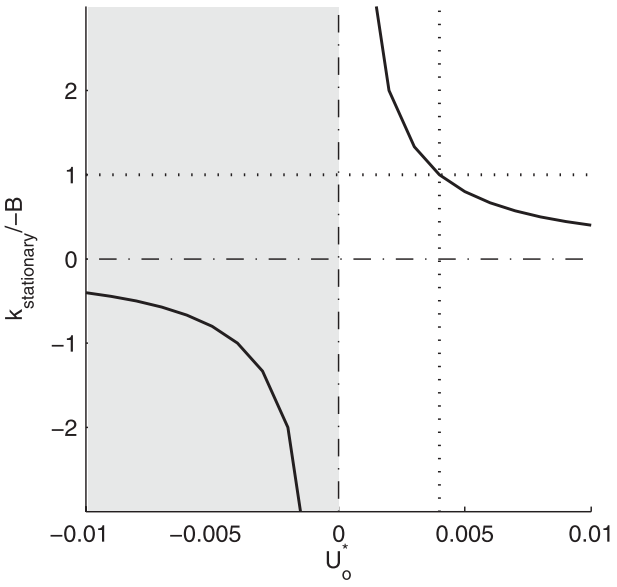

FIG. 13. The dependence of the zonal wavenumber of the stationary wave $k_{\text{stationary}}$, normalized by the optimal wavenumber B on U_o obtained from the condition $c_{\text{phase}_x} + U_o = 0$. Negative values of $k/-B$ are not permitted because westward background flows cannot arrest the Rossby waves' westward phase propagation (gray shading). The optimal response is achieved when U_o arrests the optimal wave with $|k| = B$ (dotted lines).

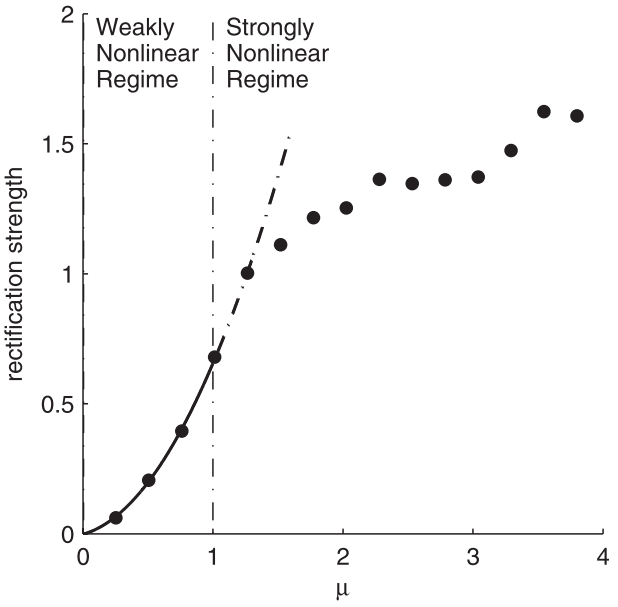

FIG. 14. Dependence of rectification strength on wave steepness/forcing amplitude for the typical case. The transition between a quadratic dependence of rectification strength on μ in the vicinity of μ = unity to a much slower rate of increase defines the transition between weakly and strongly nonlinear regimes.

changing response can be understood by considering the rectification efficiency of the given waves that are selected by the parameters of the problem. Varying U_o is a means of varying the spectrum of excited waves (by modifying the dispersion relation) but more critically is also a means to vary which wave in the excited spectrum is rendered stationary, and we find that rectification efficiency depends on the suitability of the stationary wave for rectification. Consideration of the zonal wavenumber of the stationary wave $k_{\text{stationary}}$, as a function of U_o obtained from the condition $c_{\text{phase}_x} + U_o = 0$, where c_{phase_x} is the net zonal phase speed of the forced wave, yields $k_{\text{stationary}} = \omega/-U_o$ or equivalently $k_{\text{stationary}}/B = 2\omega^2/U_o\beta$ (Fig. 13). Consistent with the fact that westward background flows cannot arrest Rossby waves' westward phase propagation, for westward background flows ($U_o < 0$) no wave is rendered stationary (because negative values of $k/-B$ are not permitted). Short waves with $k/-B > 1$ and eastward group velocities are arrested for weak eastward background flows ($0 < U_o < 2\omega^2/\beta$), whereas long waves with $k/-B < 1$ and fast westward group velocities are arrested for strong eastward background flows ($U_o > 2\omega^2/\beta$). The peak response occurs when the optimal wave with $k = -B$ is rendered stationary by the background flow, a condition that is satisfied for $U_o = -c_{\text{phase}_x}(k = -B) = 2\omega^2/\beta$. The asymmetry in the rate of change of rectification response seen in Fig. 12 for $U_o < -c_{\text{phase}_x}(k = -B)$ versus $U_o > -c_{\text{phase}_x}(k = -B)$ reflects the asymmetry in the rate of change of the zonal wavenumber of the stationary wave with respect to U_o for these two cases.

5. Extension to the strongly nonlinear regime

Results from numerical tests varying the wave nonlinearity μ via increasing the forcing amplitude A confirm the analytical prediction of a quadratic dependence of mean flow strength on A for small values of A. This dependence, however, is observed to break down as the forcing amplitude is increased (Fig. 14). Beyond this critical value, in a regime where the degree of nonlinearity is large enough that the weakly nonlinear classification is no longer valid, the mean flow response shows signs of saturation, increasing much more slowly with an increase in nonlinearity/forcing amplitude. This qualitative change in behavior in the mean flow response is consistent with the laboratory results of Whitehead (1975). Despite this systematic change of behavior however, examination of both the wave fields and the time-mean rectified flow for the weakly nonlinear and strongly nonlinear cases remain qualitatively similar in many respects (Fig. 15).

A helpful way to understand rectification in the strongly nonlinear regime is via the same interpretation in terms of the rectification efficiency of a given spectrum of linear

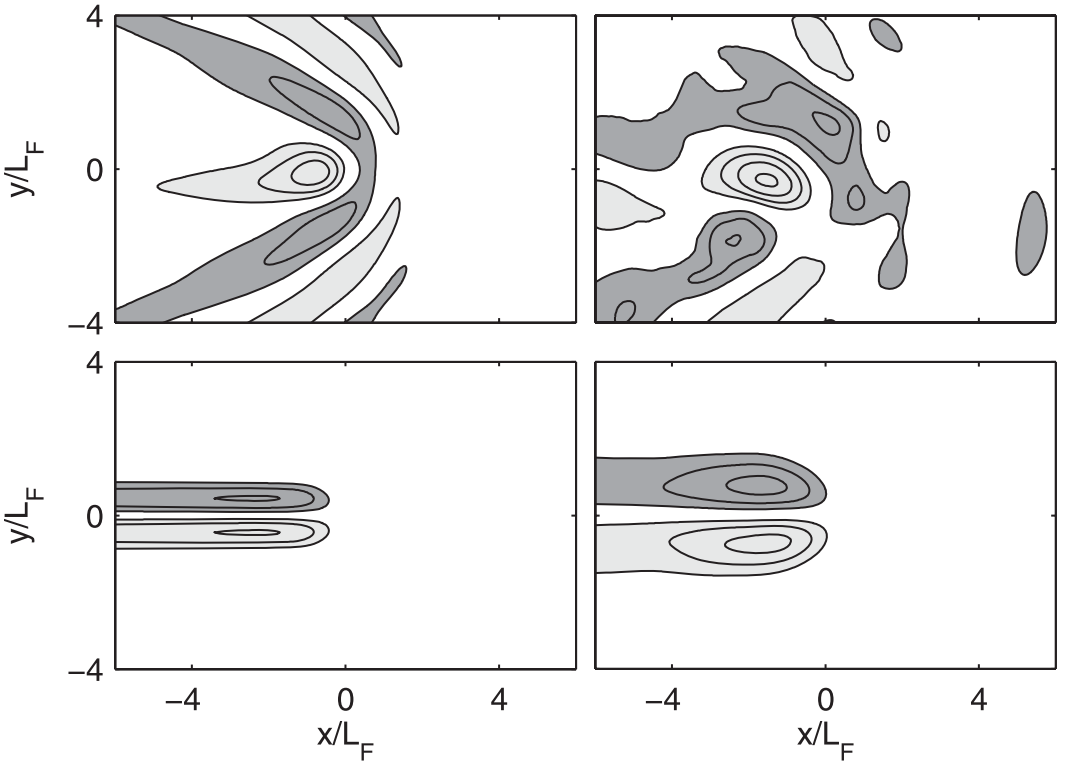

FIG. 15. A comparison of (top) wave fields (as visualized by snapshots of the instantaneous streamfunction) and (bottom) their associated time-mean rectified flows (as visualized by the time-mean streamfunction) for (left) the weakly nonlinear case ($\mu = 0.25$) versus (right) the strongly nonlinear case ($\mu = 2.5$). Contours are an order of magnitude larger in the strongly nonlinear case fields.

Rossby waves developed in the weakly nonlinear case with the addition of a mean flow and its associated mean flow effects. This latter addition is required as a consequence of the rectified mean flow now being sufficiently strong that the mean flow advection and the interaction between the waves and the mean flow are significant. These effects will be much more complicated than the case of a uniform mean background flow not only because the mean flow strength will be a direct function of the rectification efficiency, but also because the feedback it will have on the waves' ability to rectify will have important spatial dependence. This may include making a significant contribution to the effective background PV gradient through which the waves are propagating, as well as competing with the waves' intrinsic propagation. Despite this complexity, however, we find that the net effect of the mean flow's role is to counteract or reduce the ability of the waves/eddies to rectify. It is this counteracting effect that results in the saturation in the mean flow strength at large forcing amplitudes that is observed.

To illustrate, first consider the time-mean PV balance for typical weakly nonlinear and strongly nonlinear cases (Fig. 16). In the weakly nonlinear case, consistent with the simulations of HR83, the balance is predominantly a two-term one between the eddy potential vorticity flux divergence $[\overline{J(\psi', q')}]$ and the planetary vorticity flux divergence $(\beta\overline{v})$ (the so-called eddy Sverdrup balance). Mean meridional motions (northward north of the plunger and southward south of the plunger) are generated to produce the planetary vorticity flux divergence required to balance the eddy potential vorticity flux divergence. In the strongly nonlinear case, however, as a result of the mean zonal flows generated by the rectification becoming sufficiently strong, the time-mean potential vorticity balance becomes three way, because now the contribution of the mean relative vorticity flux $[J(\overline{\psi}, \overline{\zeta})]$ is also significant. At the latitudes of the time-mean westward recirculations, the mean relative vorticity flux divergence has the same sign as the eddy potential vorticity flux divergence and augments the eddy effect; however, inside the time-mean jet, the mean relative vorticity flux divergence has the opposite sign to its eddy counterpart and hence counteracts its effects there. As a consequence, the mean meridional velocity required to balance the eddy flux divergence does not have to be as large as that predicted by the quadratic trend valid in the weakly nonlinear regime, and the strength of the

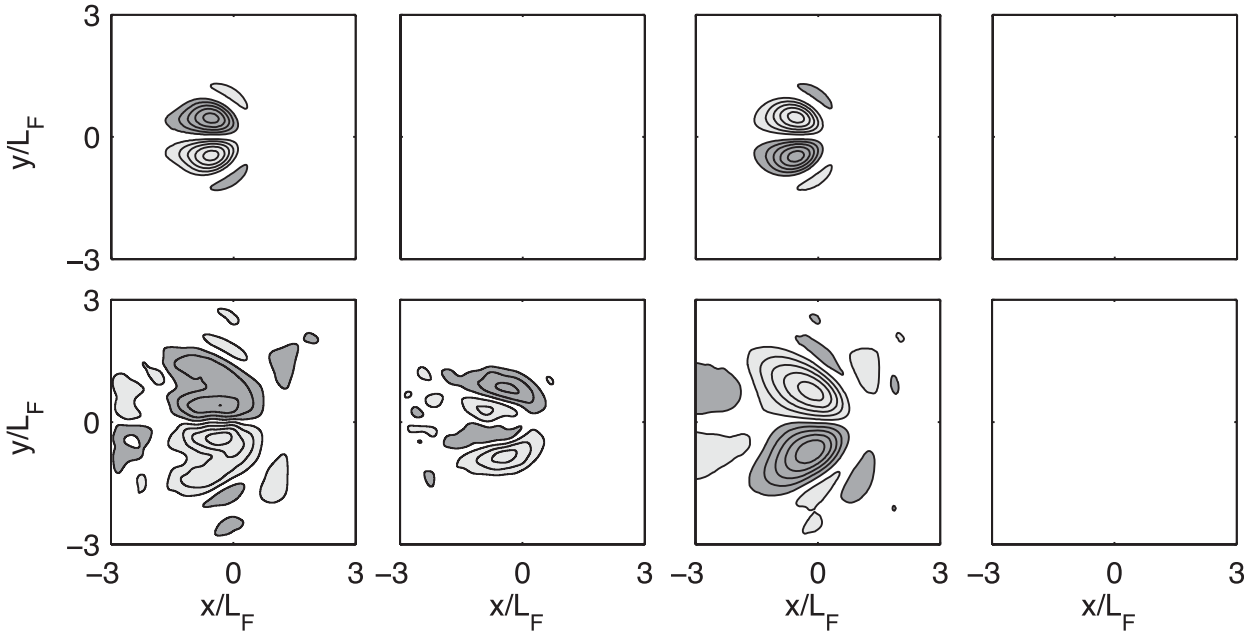

FIG. 16. The time-mean potential vorticity balance, (individual terms shown left–right) $\overline{J(\psi', q')} + J(\overline{\psi}, \overline{\zeta}) + \beta^* \overline{v} = -R\overline{q}$, for (top) the weakly nonlinear case versus (bottom) the strongly nonlinear case. Values of μ for the weakly and strongly nonlinear cases are as in Fig. 15. Contours are an order of magnitude larger in the strongly nonlinear case fields.

recirculations grows less quickly than in the weakly forced case. A nonzero mean PV flux divergence implies that PV is not homogenized in the vicinity of the forcing even in cases of large-amplitude forcing. This is confirmed via visualization of the time-mean PV field itself, which reveals that, although the mean PV gradient is reduced by forcing with large amplitude, PV is not homogenized in the vicinity of the forcing for the range of forcing amplitudes considered (Fig. 17). As such, saturation in rectification efficiency as illustrated in Fig. 14 occurs well before the limit of complete PV mixing in the near field of the forcing. This gives further support to the hypothesis that mean flow effects, not PV homogenization, underpin the saturation observed.

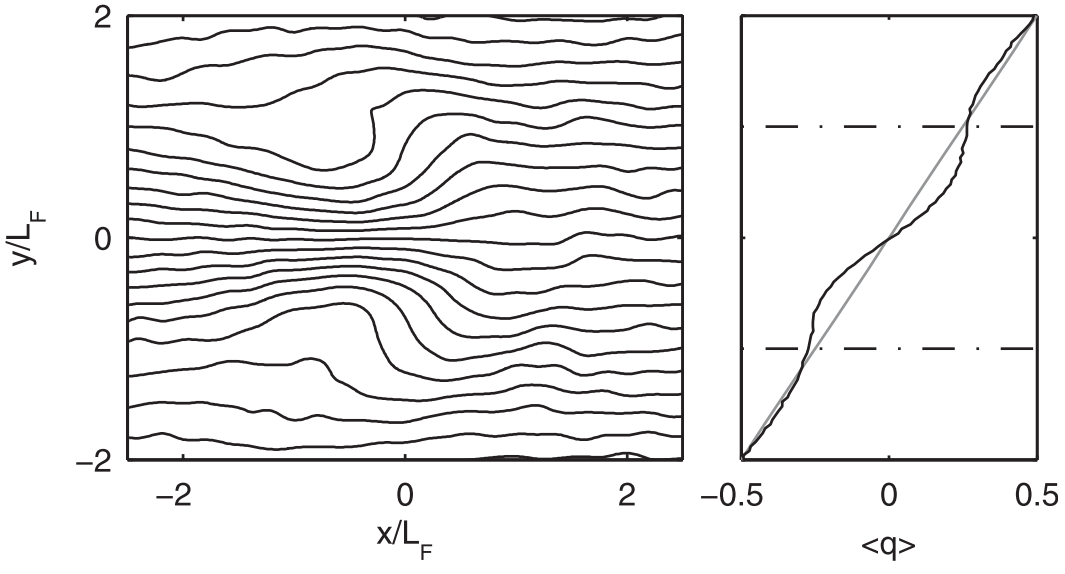

FIG. 17. (left) Contours of the time-mean PV field for the most nonlinear simulation considered ($\mu = 4.0$). (right) The meridional profile of time-mean PV at $x = 0$ for the weakly nonlinear ($\mu = 0.25$) (gray) and most strongly nonlinear ($\mu = 4.0$) (black) cases. The dashed–dotted lines indicate the meridional extent of the plunger radius.

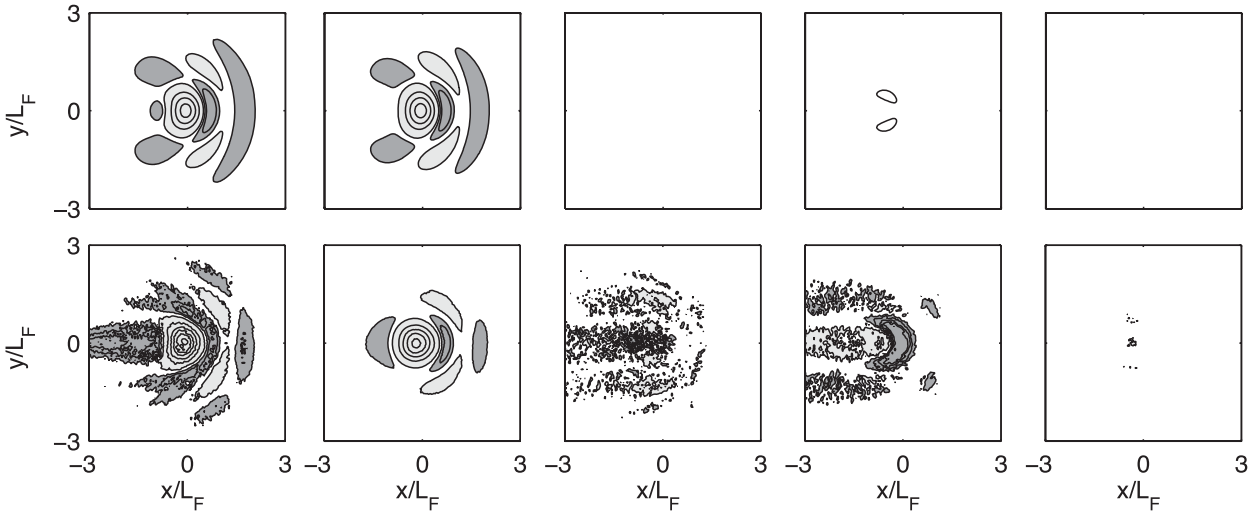

FIG. 18. As in Fig. 16, but for the time-mean eddy enstrophy budget: (left)–(right) $\overline{\mathbf{u}'q'} \cdot \nabla\overline{q}$ (the eddy vorticity flux relative to the mean PV gradient) = $\overline{F'_q q'}$ (the enstrophy injection by the forcing) $-\overline{D'_q q'}$ (the dissipation of enstrophy) $-\overline{\mathbf{u}} \cdot (\nabla q'^2/2)$ (the self-advection of eddy enstrophy) $-(\nabla \cdot \mathbf{u}' q'^2)/2$ (the advection of eddy enstrophy by the mean flow) for (top) the weakly nonlinear case versus (bottom) the strongly nonlinear case. Contours are an order of magnitude larger in the strongly nonlinear case fields.

The increasing importance of mean flow advection for increasing nonlinearity is also seen in the eddy enstrophy balance for the two cases. In the weakly nonlinear case, an up-gradient eddy vorticity transport is achieved by a dominant enstrophy budget balance in the vicinity of the forcing between the up-gradient eddy flux of potential vorticity $\overline{\mathbf{u}'q'} \cdot \nabla\overline{q}$ and the enstrophy injection by the forcing $\overline{F'_q q'}$ (Fig. 18, top). In the strongly nonlinear case, however (Fig. 18, bottom), although the dominant balance is unchanged, the mean advection of eddy enstrophy $\overline{\mathbf{u}} \cdot (\nabla q'^2/2)$ and to a lesser extent dissipation $\overline{D'_q q'}$ also play nonnegligible roles. In particular, a negative contribution by mean flow advection in the vicinity of the forcing acts to remove enstrophy supplied by the forcing. As such, it acts to reduce the rectification strength from that which would be achieved in the absence of advection for a given forcing strength.

Finally, mean flow interaction in the strongly nonlinear case is also important in the eddy zonal momentum flux convergence field (Fig. 19). In the weakly nonlinear case (Fig. 19, left), the regions of zonal momentum flux divergence occur north and south of the forcing latitude and result from the waves radiating away from the forcing. As such, because of the separation in latitude of the regions of momentum flux divergence and convergence, the waves/eddies are effective at driving the westward recirculations. In the strongly nonlinear case (Fig. 19, right), however, similar to the case of a strong eastward mean background flow, the main source of momentum flux divergence now lies on the jet axis west of the forcing, here resulting from the mean jet "running into" the westward-propagating waves. We note that this change in the orientation of the eddy momentum flux is consistent with a change in the wave population in the vicinity of the forcing toward shorter horizontal wavelengths, as would be expected if the eddy-induced flow was now competing with the waves' westward propagation. The eddy momentum flux divergence acts now not to accelerate westward flows but instead to decelerate the mean eastward jet, and rectification efficiency is reduced as a result.

6. Discussion

To close, we consider the relevance of the results described here to oceanic applications. It is challenging to obtain enough observational data to accurately calculate eddy statistics; as a consequence, diagnostic studies of the relation between the time-mean or low-frequency state and eddies using direct observations of the ocean circulation have been rare. Some attempts, however, have been made with limited data on regional scales, and some do observe signatures of eddy–mean flow interactions consistent with the mechanism discussed here. Thompson (1977, 1978), for example, suggests that eddies may be playing a role in the net driving of the mean Gulf Stream jet and its inshore counter current by transferring momentum between the jet and the countercurrent via a pattern of momentum flux convergences and divergences consistent with the process studied here. In an examination of eddy effects on abyssal ocean dynamics also in the region of the Gulf Stream, Hogg (1993) argues

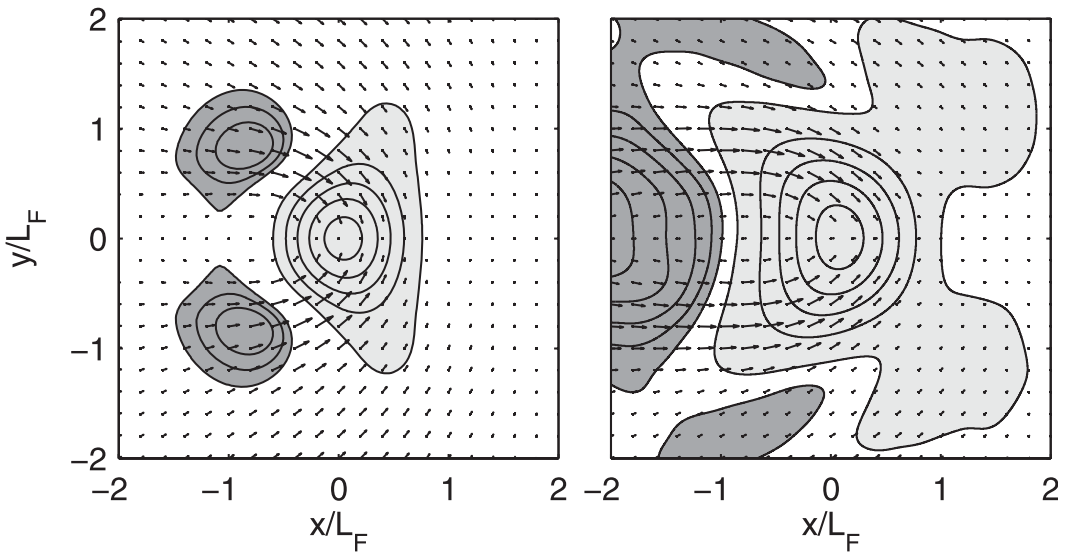

FIG. 19. A comparison of the time-mean zonal eddy force {the time-mean eddy zonal momentum flux convergence, $-[(\partial/\partial x)\overline{u'u'} + (\partial/\partial y)\overline{u'v'}]$} (contours) with eddy zonal momentum transport ($\overline{u'u'}\mathbf{i} + \overline{u'v'}\mathbf{j}$) (vectors) overlaid for (left) the weakly nonlinear versus (right) the strongly nonlinear cases. Values of μ are as in Fig. 15. Contours are an order of magnitude larger in the strongly nonlinear case field.

that the eddy relative vorticity flux divergence is of the right sign and order of magnitude to drive a recirculation of the observed strength. Other analyses in the Gulf Stream (e.g., Hall 1986; Dewar and Bane 1989; Cronin 1996) suggest a more complicated picture of the eddy forcing that appears at some times and locations consistent with the rectification mechanism considered here (e.g., Hall 1986) but at others is instead typical of baroclinic (e.g., Cronin 1996) or barotropic (e.g., Dewar and Bane 1989, at 68.8°W) instability processes. We conjecture that, in WBC jets, rectification will be important at locations and times where wave radiation dominates over instability processes and as such is more likely in the far field of jets (e.g., Malanotte-Rizzoli et al. 1987), in the downstream regions of WBC jet extensions (see Waterman and Jayne 2011), and at times not dominated by meander formation events (as in Cronin 1996).

The parameter values explored in this study are realistic and relevant to synoptic scales of, for example, a strong localized wind stress or a localized concentration of eddy activity as, for example, generated by mean flow instability. The magnitude of the mean flow generated, on the order of the dimensional equivalent of a few centimeters per second for small-amplitude forcing and up to the dimensional equivalent of tens of centimeters per second for large-amplitude forcing, could be significant to the oceanic circulation, especially below the thermocline where the mean velocities are small. It is sufficient for instance to account for the mean deep recirculation gyre velocities observed, typically 2–10 cm s^{-1} in the Gulf Stream (Schmitz 1980; Hogg et al. 1986) and 2–4 cm s^{-1} in the Kuroshio Extension (Jayne et al. 2009). Our results suggest that in order for rectification to be efficient, a very special relationship between the forcing and flow parameters must exist such that the forcing selects meridionally propagating waves; however, this is for the case in which only one forcing frequency is applied. In a more realistic setting, the forcing would likely include a broad range of frequencies and the rectification mechanism would then select the forcing power around the resonant frequency and use that to drive the mean rectified flow. In this way, we would expect the rectified flow to reflect the forcing energy available in the suitable selection of the frequency–wavenumber forcing spectra. Nevertheless, significant stratification or a background mean flow could still render the mechanism ineffective in practice. Hence, for this mechanism to be important in the ocean, it requires a sufficiently well-matched set of forcing and environmental parameters, as well as weak stratification and a weak or well-matched background flow. The latter two requirements make rectification to be likely more significant for abyssal as opposed to above-thermocline flows. The incomplete PV homogenization seen even in the strongly nonlinear cases illustrates that the range of forcing amplitudes considered in this study do not reach the point of violent stirring, which does occur in nature (Rhines and Schopp 1991, and references therein). As such, the relevance of larger forcing amplitudes and/or

other processes leading to eddy mixing in the real ocean should be considered.

Mean flows driven by the mechanism of rectification would not be represented in a general circulation model with eddy effects parameterized simply as down-gradient diffusion. For recirculations in WBC jet systems, driven likely by a combination of inertial forcing and eddy driving via the mechanism proposed here, this could have significant impacts on WBC jet vertical structure and transport with important climatic implications for the oceanic meridional heat transport. We find in a subsequent study examining the downstream equilibration of an unstable jet (as would be relevant to a separated western boundary current) that this ''plunger like'' mechanism is indeed a useful model for the effect of the eddies downstream of jet stabilization, where eddies are responsible for driving weakly depth-dependent recirculations that add significantly to the jet's time-mean transport. See Waterman and Jayne (2011) for further discussion.

Acknowledgments. The authors would like to gratefully acknowledge useful discussions with Pavel Berloff, Joseph Pedlosky, and John Whitehead, as well as very insightful reviews provided by Peter Rhines. SW was supported by the MIT Presidential Fellowship and the National Science Foundation under Grants OCE-022 0161 and OCE-0825550. The financial assistance of the Houghton Fund, the MIT Student Assistance Fund, and WHOI Academic Programs is also gratefully acknowledged. SRJ was supported by the National Science Foundation under Grants OCE-0220161 and OCE-0849808. The model integrations were performed at the National Center for Atmospheric Research, which is supported by the National Science Foundation.

REFERENCES

Arakawa, A., 1966: Computational design for long-term numerical integration of the equations of fluid motion: Part I: Two-dimensional incompressible flow. *J. Comput. Phys.,* **1,** 119–145.

Bower, A. S., and N. G. Hogg, 1996: Structure of the Gulf Stream and its recirculations at 55°W. *J. Phys. Oceanogr.,* **26,** 1002–1022.

Chen, S., B. Qiu, and P. Hacker, 2007: Profiling float measurements of the recirculation gyre south of the Kuroshio Extension in May to November 2004. *J. Geophys. Res.,* **112,** C05023, doi:10.1029/2006JC004005.

Cronin, M., 1996: Eddy-mean flow interaction in the Gulf Stream at 68°W. Part II: Eddy forcing on the time-mean flow. *J. Phys. Oceanogr.,* **26,** 2132–2151.

Dewar, W. K., and J. M. Bane, 1989: Gulf Stream dynamics. Part II: Eddy energetics at 73°W. *J. Phys. Oceanogr.,* **19,** 1574–1587.

Dritschel, D. G., and M. E. McIntyre, 2008: Multiple jets as PV staircases: The Phillips effect and the resilience of eddy transport barriers. *J. Atmos. Sci.,* **65,** 855–874.

Durran, D. R., 1991: The third-order Adams–Bashforth method: An attractive alternative to leapfrog time differencing. *Mon. Wea. Rev.,* **119,** 702–720.

Flierl, G. R., P. Malanotte-Rizzoli, and N. J. Zabusky, 1987: Nonlinear waves and coherent vortex structures in barotropic β-plane jets. *J. Phys. Oceanogr.,* **17,** 1408–1438.

Haidvogel, D. B., and P. B. Rhines, 1983: Waves and circulation driven by oscillatory winds in an idealized ocean basin. *Geophys. Astrophys. Fluid Dyn.,* **25,** 1–63.

Hall, M. M., 1986: Horizontal and vertical structure of the Gulf Stream velocity field at 68°W. *J. Phys. Oceanogr.,* **16,** 1814–1828.

Hogg, N. G., 1985: Evidence for baroclinic instability in the Gulf Stream recirculation. *Prog. Oceanogr.,* **14,** 209–229.

——, 1992: On the transport of the Gulf Stream between Cape Hatteras and the Grand Banks. *Deep-Sea Res.,* **39,** 1231–1246.

——, 1993: Toward parameterization of the eddy field near the Gulf Stream. *Deep-Sea Res.,* **40,** 2359–2376.

——, R. S. Pickart, R. M. Hendry, and W. J. Smethie Jr., 1986: The northern recirculation gyre of the Gulf Stream. *Deep-Sea Res.,* **33,** 1139–1165.

Holland, W. R., and P. B. Rhines, 1980: An example of eddy-induced ocean circulation. *J. Phys. Oceanogr.,* **10,** 1010–1031.

Hoskins, B. J., I. N. James, and G. H. White, 1983: The shape, propagation and mean-flow interaction of large-scale weather systems. *J. Atmos. Sci.,* **40,** 1595–1612.

Hsu, C. J., and R. A. Plumb, 2000: Nonaxisymmetric thermally driven circulations and upper-tropospheric monsoon dynamics. *J. Atmos. Sci.,* **57,** 1255–1276.

Huang, H., A. Kaplan, E. N. Curchitser, and N. A. Maximenko, 2007: The degree of anisotropy for mid-ocean currents from satellite observations and an eddy-permitting model simulation. *J. Geophys. Res.,* **112,** C09005, doi:10.1029/2007JC004105.

Jayne, S. R., 2006: The circulation of the North Atlantic Ocean from altimetry and the geoid. *J. Geophys. Res.,* **111,** C03005, doi:10.1029/2005JC003128.

——, and N. G. Hogg, 1999: On recirculation formed by an unstable jet. *J. Phys. Oceanogr.,* **29,** 2711–2718.

——, and Coauthors, 2009: The Kuroshio Extension and its recirculation gyres. *Deep-Sea Res. I,* **56,** 2088–2099.

Lighthill, M. J., 1967: On waves generated in dispersive systems by travelling forcing effects, with applications to the dynamics of rotating fluids. *J. Fluid Mech.,* **27,** 725–752.

Malanotte-Rizzoli, P., D. B. Haidvogel, and R. E. Young, 1987: Numerical simulation of transient boundary-forced radiation. Part I: The linear regime. *J. Phys. Oceanogr.,* **17,** 1439–1457.

Marcus, P. S., 1993: Jupiter's Great Red Spot and other vortices. *Annu. Rev. Astron. Astrophys.,* **31,** 523–573.

Maximenko, N. A., B. Bang, and H. Sasaki, 2005: Observational evidence of alternating zonal jets in the World Ocean. *Geophys. Res. Lett.,* **32,** L12607, doi:10.1029/2005GL022728.

Nakano, H., and H. Hasumi, 2005: A series of zonal jets embedded in the broad zonal flows in the Pacific obtained in eddy-permitting ocean general circulation models. *J. Phys. Oceanogr.,* **35,** 474–488.

Pedlosky, J., 1965: A study of the time dependent ocean circulation. *J. Atmos. Sci.,* **22,** 267–272.

Plumb, R. A., 1985: On the three-dimensional propagation of stationary waves. *J. Atmos. Sci.,* **42,** 217–229.

——, 1986: Three-dimensional propagation of transient quasi-geostrophic eddies and its relationship with the eddy forcing of the time-mean flow. *J. Atmos. Sci.,* **43,** 1657–1678.

Rhines, P. B., 1975: Waves and turbulence on a beta-plane. *J. Fluid Mech.,* **69,** 417–443.

——, 1977: The dynamics of unsteady currents. *The Sea,* E. Goldberg, Ed., John Wiley and Sons, Inc., Vol. 6, 189–318.

——, 1979: Geostrophic turbulence. *Annu. Rev. Fluid Mech.,* **11,** 401–441.

——, 1983: Lectures on geophysical fluid dynamics. *Lect. Appl. Math.,* **20,** 1–58.

——, and W. R. Holland, 1979: A theoretical discussion of eddy-driven flows. *Dyn. Atmos. Oceans,* **3,** 289–325.

——, and R. Schopp, 1991: The wind-driven circulation: Quasi-geostrophic simulations and theory for nonsymmetric winds. *J. Phys. Oceanogr.,* **21,** 1428–1469.

Richards, K. J., N. A. Maximenko, F. O. Bryan, and H. Sasaki, 2006: Zonal jets in the Pacific Ocean. *Geophys. Res. Lett.,* **33,** L03 605.

Schmitz, W. J., 1980: Weakly depth-dependent segments of the North Atlantic circulation. *J. Mar. Res.,* **38,** 111–133.

Thompson, R. O. R. Y., 1971: Why there is an intense eastward current in the North Atlantic but not in the South Atlantic? *J. Phys. Oceanogr.,* **1,** 235–237.

——, 1977: Observations of Rossby waves near site D. *Prog. Oceanogr.,* **7,** 1–28.

——, 1978: Reynolds stress and deep counter-currents near the Gulf Stream. *J. Mar. Res.,* **36,** 611–615.

Trenberth, K. E., 1986: An assessment of the impact of transient eddies on the zonal flow during a blocking episode using localized Eliassen-Palm flux diagnostics. *J. Atmos. Sci.,* **43,** 2070–2087.

Vallis, G. K., 2006: *Atmospheric and Oceanic Fluid Dynamics: Fundamentals and Large-Scale Circulation*. Cambridge University Press, 745 pp.

Veronis, G., 1966: Wind-driven circulation. Part 2: Numerical solutions of the non-linear problem. *Deep-Sea Res.,* **13,** 31–55.

Waterman, S., and S. R. Jayne, 2011: Eddy-mean flow interactions in the along-stream development of a western boundary current jet: An idealized model study. *J. Phys. Oceanogr.,* **41,** 682–707.

Whitehead, J., 1975: Mean flow driven by circulation on a beta-plane. *Tellus,* **27,** 358–364.

Williams, G. P., 1979: Planetary circulations: 2. The Jovian quasi-geostrophic regime. *J. Atmos. Sci.,* **36,** 932–968.